ACS Sustainable Chemistry & Engineering

Research Article

pubs.acs.org/journal/ascecg

# Shell Structure Control of PPy-Modified CuO Composite Nanoleaves for Lithium Batteries with Improved Cyclic Performance

Zhigang Yin,[†,‡] Wenbin Fan,[†] Yunhai Ding,[†] Jiaxin Li,[†] Lunhui Guan,*[,†] and Qingdong Zheng*[,†]

[†]State Key Laboratory of Structural Chemistry, Fujian Institute of Research on the Structure of Matter, Chinese Academy of Sciences, 155 Yangqiao Road West, Fuzhou, Fujian 350002, China

[‡]University of Chinese Academy of Sciences, 19 Yuquan Road, Beijing 100049, China

Supporting Information

**ABSTRACT:** Polypyrrole (PPy)-modified CuO nanocomposites (NCs) with various shell structures have been synthesized by controlling the polymerization time of pyrrole in the presence of leaf-like CuO nanobelts (NBs) as wire templates. The synthesized CuO/PPy NCs and CuO NBs are characterized by XRD, FT−IR, TGA, SEM, TEM, STEM, and EDX line analysis/elemental mapping. The formation mechanism of CuO/PPy core−shell NCs is also illustrated. Electrochemical lithium-storage properties of all the products are evaluated by using them as anode materials for Li-ion batteries (LIBs). It is found that the polymerization time of pyrrole plays a significant role in affecting the shell structures and subsequent lithium-storage properties of the hybrid CuO/PPy NCs. With the extension of polymerization time, CuO/PPy NCs gradually form typical core−shell structures, where the doped PPy with increasing content is steadily and uniformly coated on the CuO surface. Correspondingly, the discharge/charge capacity and cyclic durability of CuO/PPy NCs are significantly enhanced. For the core−shell NCs made by the 3 h polymerization, a greatly improved initial capacity of 1114 mAh $g^{-1}$ and a high reversible capacity of 760 mAh $g^{-1}$ are achieved, which are much better than those of the bare CuO NBs and the NCs without core−shell structures. The improved performance of core−shell CuO/PPy NCs can be attributed to their advantageous structure features that buffer volume variations of the rigid CuO, allow short Li-ion diffusion length, form good interface interaction between PPy and CuO for charge transfer, and avoid direct contacts between CuO and electrolytes during charge−discharge processes. This study indicates that the structural tuning of polymer/metal oxide composites by controlling the polymerization time is a simple and promising way to improve the electrode performance of NCs for energy storage.

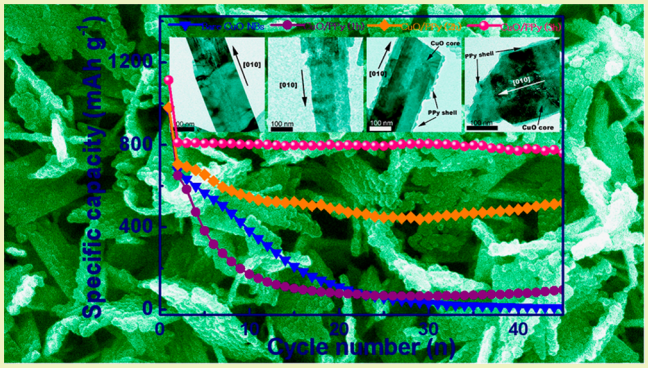


**KEYWORDS:** *Conducting polymers, Metal oxides, Composite materials, Polymerization, Green synthesis, Electrochemical properties, Lithium-ion batteries*

## INTRODUCTION

As a new generation energy storage device, lithium-ion batteries (LIBs) have been extensively used in smart phones, laptop computers, digital cameras, wireless home appliances, and other portable electronic products, which play an important role in promoting an efficient use of clean energies.[1,2] Usually, a LIB device contains two electrodes (anode and cathode), an electrolyte, and a separator. In addition to device engineering, each component material used in LIBs has great influence on battery performance.[3,4] Particularly for the electrode materials, they play a key role in electrochemical lithium storage of LIBs, which essentially affect battery performance such as the voltage, charge/discharge capacity, rate ability, and cycle stability.[5−7] Therefore, how to facilely and efficiently synthesize electrode materials with good electrical/electrochemical properties for high performance LIBs has far-reaching significance for future energy storage applications.

In recent years, the ever-increasing and urgent necessities of electric vehicles (EVs) and hybrid EVs (HEVs) have promoted worldwide studies on developing LIBs with large capacities, high power densities, and good cyclic stabilities.[8−11] Because the dominant commercial graphite anode material has almost reached its theoretical capacity (372 mAh $g^{-1}$), developing novel anodes with higher capacity and superior stability has become an urgent task. Transition metal oxides ($M_xO_y$, M = Fe, Co, Ni, Cu, etc.) have attracted much attention as potential alternative anodes for next generation LIBs owing to their much larger capacities compared with those of graphite anodes.[12−17] Especially, copper oxide (CuO) has been widely used as an anode material for LIBs due to its high theoretical capacity, low cost, natural abundance, and environmental

Received: November 26, 2014
Revised: January 9, 2015
Published: January 21, 2015





DOI: 10.1021/sc500755d
ACS Sustainable Chem. Eng. 2015, 3, 507−517

benignity.[18,19] However, the main challenge for using CuO as active anodes is their drastic volume changes during repeated charge−discharge processes, resulting in electrode pulverization and rapid capacity fading. Besides, the intrinsically low conductivity of CuO is not favorable for charge-transport under working conditions, which also limits the use of anodes in LIBs. The reasons mentioned above have led to the final low capacity and poor cyclic durability of LIBs with bare CuO anodes. These problems are also the general challenges existing in most metal oxide electrodes,[14,20] which hinder their commercial utilization for LIBs.

To circumvent the above issues, many research teams have paid attention to the improvement of cyclic performance by designing CuO anodes with optimized particle sizes and shapes.[21−23] So far, various nanostructural CuO materials such as dots, cubes, rods/wires, plates, and cog-like or sphere-like architectures have been synthesized and used in LIBs with improved performances.[19,24−30] Among them, one-dimensional (1D) nanoscale CuO anodes with unique anisotropic structures exhibit improved cyclabilities, efficiencies, and rate capabilities, even at high current rates, due to the short diffusion length of Li-ions and large surface reaction sites of their electroactive components and the increased charge-transfer properties of CuO electrodes as well.[25,31−33] However, 1D CuO nanomaterials still have some shortcomings such as poor thermodynamic stability and pulverization/aggregation because of their large surface area and high surface energy, as well as the mechanical rigidity and low conductivity in nature. The incorporation of carbon materials (e.g., carbon nanotubes and graphene) as functional counterparts into CuO nanomaterials is one good method to overcome the poor capacity retention of these anodes, owing to the high conductivity and small volume changes of carbon materials during $Li^+$ insertion/extraction.[34−37] Another effective strategy to improve the electrochemical properties of metal oxide nanomaterials is to effectively enhance their structural stability by introducing organic conducting polymers, such as polypyrrole (PPy) and polyaniline (PANI), to serve as soft conducting coating layers and/or matrices. As we highlighted in a recent review article,[38] conducting polymers can serve as a buffering space that accommodates volume variations and improves the cyclability of metal oxide electrodes for various energy storage devices due to their excellent mechanical flexibility, high conductivity, and good electrochemical stability. Similarly, improved performance has also been demonstrated by other groups with the use of conducting polymers to modify NiO, $MnO_2$, $SnO_2$ and $Fe_3O_4$ anodes.[39−42] However, there are few reports employing conducting polymers to enhance the performance of CuO anodes.[43]

In our preliminary work, we presented novel CuO/PPy nanocomposites (NCs) for efficient lithium storage, demonstrating the first example of conducting polymers hybridized with CuO as anodes in LIBs.[43] The NCs showed good initial and reversible capacities of 991 and 613 mAh $g^{-1}$, respectively. However, the influence of PPy surface modification on the structures of CuO/PPy NCs is still not clear, and the relationship between the shell structure and charge/discharge properties of CuO/PPy NCs also needs to be investigated in depth. Herein, we study the effects of the polymerization time of pyrrole on structural features and lithium-storage properties of hybrid CuO/PPy NCs. The structures of the products are comprehensively characterized. The relationships between the structures of the NCs and their charge−discharge properties are investigated in detail. The greatly improved lithium-storage properties of the optimized core−shell CuO/PPy NCs are discussed in comparison with those of bare CuO nanobelts (NBs) and CuO/PPy NCs without core−shell structures. We find that the structural tuning of CuO/PPy NCs by facilely controlling the polymerization time significantly improves discharge/charge capacities and cyclic performances in LIBs, which is mainly due to the changes in shell structure features in the hybrid products.

## EXPERIMENTAL SECTION

**Materials.** Copper acetate monohydrate ($Cu(CH_3COO)_2{\cdot}H_2O$), sodium hydroxide (NaOH), pyrrole (Py), ammonium persulfate (APS, $(NH_4)_2S_2O_8$), sodium dodecyl sulfate (SDS), hydrochloric acid (HCl) solution, and anhydrous ethanol were purchased from Sinopharm Chemical Reagent Co., Ltd. and used as received. Deionized water was obtained in our laboratory by using a deionizer system (P10-W, Kertone Water Treatment Co., Ltd.). Other materials and reagents were purchased from Sigma-Aldrich, Inc. or Sinopharm Chemical Reagent Co., Ltd. All chemicals were of analytical grade and used without further purification.

**Preparation of Samples.** Leaf-like CuO NBs were similarly fabricated by a solution phase growth route described in the previous report.[43] Typically, 0.5 M aqueous solution of $Cu(CH_3COO)_2{\cdot}H_2O$ and 2.0 M NaOH solution were mixed together to produce massive $Cu(OH)_2$ precipitates at room temperature. The obtained suspension was then preserved in a 60 °C water bath for 6 h to form leaf-like CuO NBs. The black products were then collected by centrifugation and sequentially washed with deionized water and anhydrous ethanol several times. The purified products were equally divided into two parts, where one part was dried under vacuum at 50 °C for 24 h to obtain the final CuO sample and the other was further employed to fabricate PPy-modified CuO NCs.

For the preparation of hybrid CuO/PPy NCs, the leaf-like CuO NBs synthesized above as wire templates were dispersed into deionized water containing a small amount of SDS under ultrasonication for 10 min, followed by vigorous stirring for 12 h at room temperature. Then, a pyrrole monomer (0.5 mmol) and 1 M HCl aqueous solution (0.5 mL) as a dopant were successively added into the suspension. This solution was further vigorously stirred for 30 min. Subsequently, a freshly prepared 0.1 M APS aqueous solution (5 mL) was dropwise added into the system as an oxidant to start the polymerization process in an ice/water bath under constant mild stirring. The polymerization reaction was carried out with controlled polymerization times (1, 2, and 3 h) of pyrrole. The resulting three types of hybrid CuO/PPy nanocomposite products were obtained by filtration and rinsed with deionized water and anhydrous ethanol several times. Finally, the samples were dried in vacuum at 50 °C for 24 h.

**Characterization of Samples.** The crystalline structures of the CuO and CuO/PPy samples were examined by X-ray powder diffraction (XRD) with a Rigaku Miniflex II diffractometer (Cu K$\alpha$ radiation, 30 kV, 15 mA). Morphologies and structure features of the obtained products were characterized by scanning electron microscopy (SEM, JSM-6700F), transmission electron microscopy, and scanning transmission electron microscopy (TEM and STEM, FEI Tecani G2 F20). Note that the SEM and STEM systems were equipped with energy-dispersive X-ray (EDX) spectroscopy units. Fourier transform−infrared (FT−IR) spectra of the samples were recorded on a VERTEX70 spectrometer (KBr pellets). The contents of PPy in hybrid CuO/PPy samples were estimated by using thermal gravimetric analysis (TGA) equipped with a STARe System (NETZSCH STA449C) from 40 to 1000 °C at 10 °C $min^{-1}$ in air.

**Cell Assembly and Electrochemical Measurements.** Electrochemical lithium-storage properties of the synthesized products were measured by using CR2025 coin-type test cells assembled in a dry argon-filled glovebox. To fabricate the working electrode, a slurry consisting of 80 wt % active materials, 10 wt % conductive materials


DOI: 10.1021/sc500755d
ACS Sustainable Chem. Eng. 2015, 3, 507−517

(acetylene black), and 10 wt % polymer binders (polyvinylidene difluoride, PVDF) dissolved in 1-methyl-2-pyrrolidinone was casted on a copper foil, drying at 80 °C under vacuum for 24 h. The loading of active materials is typically about 1.3 ± 0.2 mg $cm^{-2}$. Lithium sheets were used as both the counter and reference electrodes, while a Celgard 2300 membrane was employed as a separator. The electrolyte was a solution of 1 M $LiPF_6$ in ethylene carbonate/dimethyl carbonate/ethylmethyl carbonate (1:1:1 in volume). With a galvanostatic mode, the assembled cells were tested (discharging, charging, and cycling) by a LAND battery system at 30 °C within a voltage range of 0.05−3.00 V (vs. $Li/Li^+$). Note that the mass of PPy was included when calculating the specific capacity of hybrid CuO/PPy NCs.

## RESULTS AND DISCUSSION

**XRD Characterization of Samples.** XRD analysis was used to determine the crystalline structure and phase of the synthesized products. Figure 1 shows the XRD patterns of the

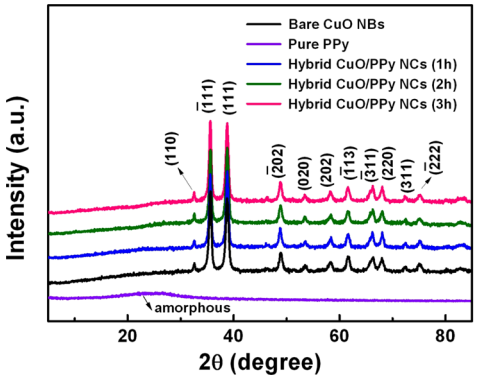


**Figure 1.** XRD patterns of bare CuO NBs, hybrid CuO/PPy NCs with controlled polymerization times, and pure PPy made by etching CuO in hybrid NCs.

bare CuO NBs, hybrid CuO/PPy NCs with controlled polymerization times (1, 2, and 3 h), and pure PPy made by etching CuO in the hybrid NCs. All the characteristic diffraction peaks of the CuO and CuO/PPy samples correspond well with normal crystallographic data of CuO (JCPDS No. 05-0661, space group $C2/c$).[35] The structure is a nanocrystalline monoclinic phase with diffraction peaks at 32.5°, 35.6°, 38.8°, 48.8°, 53.4°, 58.2°, 61.6°, 66.3°, and 68.1°, which are ascribed to the (110), ($\bar{1}$11), (111), ($\bar{2}$02), (020), (202), ($\bar{1}$13), ($\bar{3}$11), and (220) planes of monoclinic CuO, respectively. The positions of all the sharp peaks are in agreement with the results reported by Qian and co-workers.[27] No other diffraction peaks from impurities such as $Cu(OH)_2$ and $Cu_2O$ are observed, suggesting high purity of the synthesized CuO NBs and CuO/PPy NCs. Consistent with the XRD analysis of CuO, the EDX spectrum in Figure S1 of the Supporting Information demonstrates that the bare CuO sample is only made of Cu and O, and its atomic ratio is close to 1:1 in stoichiometry, further confirming the purity of the CuO products. Moreover, a broad XRD peak of amorphous PPy is not clearly observed at the $2\theta$ of about 23° for the hybrid CuO/PPy samples due to its relatively weak peak intensity compared to the CuO diffraction peaks. Nevertheless, the amorphous PPy in the hybrid CuO/PPy NC is further determined by the XRD pattern of a sample prepared by removing CuO in the hybrid NCs (3 h) by etching with acid solutions.

**FT−IR Analysis of Samples.** The structure features and compositions of the synthesized CuO NBs and hybrid CuO/PPy NCs with different polymerization times were further characterized by FT−IR spectroscopy. As shown in Figure 2,

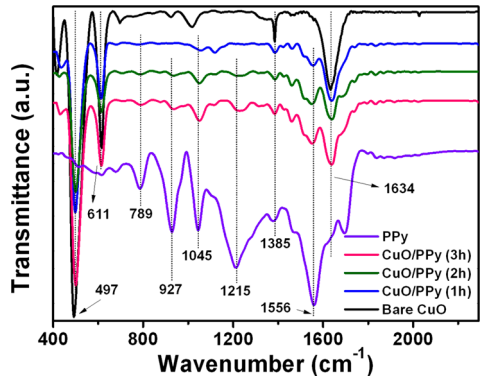


**Figure 2.** FT−IR spectra of bare CuO NBs, hybrid CuO/PPy NCs with different polymerization times, and pure PPy made by etching CuO in hybrid NCs.

there are two strong absorption bands observed at about 497 and 611 $cm^{-1}$ in the low wavenumber region for both the CuO and CuO/PPy samples, assigning to the Cu−O stretching vibration, which further proves the formation of pure-phase CuO with a monoclinic structure.[27] In comparison with the data reported, there exists some slight difference that may be caused by the changes in sample types, temperatures, and broadness of the spectra.[27] For the FT−IR spectra of all the hybrid CuO/PPy samples, the characteristic peaks centered at about 1556 and 1458 $cm^{-1}$ are due to the antisymmetric and symmetric ring-stretching modes of the PPy rings, respectively.[44] Bands at approximately 1045 and 789 $cm^{-1}$ are ascribed to the in-plane and out-of-plane vibrations of C−H deformation, respectively.[42,45] Therefore, the FT−IR results ascertain that organic PPy is formed in all three hybrid CuO/PPy NCs. Moreover, it should be noted that the strong bands near 1215 and 927 $cm^{-1}$ are assigned to the stretching vibration of doped PPy in the hybrid CuO/PPy NCs synthesized by 2 and 3 h polymerization.[45,46] By contrast, there is no apparent doping state of PPy observed in CuO/PPy NCs synthesized by the 1 h polymerization. These results further indicate that the polymerization time of pyrrole affects the doping state of synthesized PPy in CuO/PPy NCs, which will influence final structures and properties of the hybrid products. In addition to the characteristic peaks of CuO and PPy, a broad absorption band at ∼1634 $cm^{-1}$ has also been found due to the existence of water molecules in the products.[43,47] The appearance of a small absorption peak at ∼1385 $cm^{-1}$ is attributed to the presence of $CO_3^{-2}$, which is usually obtained in the FT−IR spectra when the samples were prepared in air.[47]

**TGA Results of Samples.** To determine the PPy contents in the synthesized CuO/PPy NCs, TGA of bare CuO NBs, and hybrid CuO/PPy NCs made by different polymerization times, was carried out in air from 40 to 1000 °C at a rate of 10 °C $min^{-1}$. As shown in Figure 3, the hybrid CuO/PPy samples show two-step weight loss regions. The initial weight loss from hybrid CuO/PPy NCs below 200 °C is probably due to the removal of surface hydroxyls and/or surface absorbed solvents.[42,48] The weight loss at higher temperature ranging from 200 to 1000 °C is mainly ascribed to the decomposition


DOI: 10.1021/sc500755d
ACS Sustainable Chem. Eng. 2015, 3, 507−517

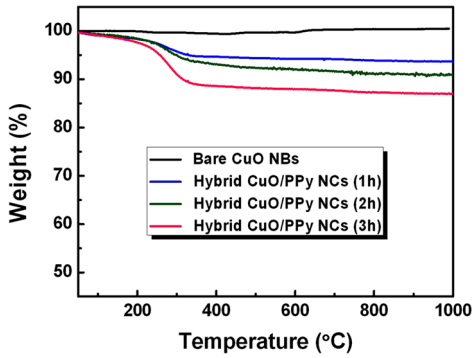


**Figure 3.** TGA curves of bare CuO NBs and three types of hybrid CuO/PPy NCs synthesized with different polymerization times.

and oxidation of PPy in air.[41] By contrast, the bare CuO sample shows almost no weight change in the whole tested temperature range. At the same time, the weight loss of the hybrid CuO/PPy NCs increases with prolonging the polymerization time of pyrrole, demonstrating the gradually increasing content of PPy in hybrid CuO/PPy NCs. According to the TGA curves, the mass fractions of PPy in the CuO/PPy samples can be estimated, which are about 5%, 8%, and 13%, for the hybrid CuO/PPy NCs synthesized with the polymerization times of 1, 2, and 3 h, respectively. The TGA results further indicate that the content of PPy in the hybrid CuO/PPy NCs can be easily tuned by controlling the polymerization time of pyrrole, which provides a simple pathway to adjust the structure and composition of the polymer−metal oxide hybrid materials.

**Morphologies and Microstructure Features of Samples.** The morphologies and sizes of CuO NBs and hybrid CuO/PPy NCs with different polymerization times were characterized by SEM measurements. As shown in Figure 4a and b, the bare CuO products are uniform leaf-like NBs with widths of approximately 20−270 nm, thicknesses of about 10−40 nm, and lengths up to hundreds of nanometers. It is also observed that the leaf-like CuO NBs have smooth surfaces and bending ends. For the hybrid CuO/PPy NCs with the polymerization times of 1, 2, and 3 h, Figure 4c, e, and g present their panoramic SEM images, respectively. The entire hybrid CuO/PPy NCs are composed of large quantities of leaf-like flexible NBs, which are overlapped and intertwined to some extent. As further shown in the magnified SEM images of Figure 4d, f, and h, the detailed morphologies and structure features of CuO/PPy NCs with different polymerization times are depicted. These high-magnification images clearly display that incorporating PPy does not change the general shape of leaf-like CuO NBs but results in the difference in the surface morphology of the hybrid products. With prolonged polymerization time, it is clearly found that the surfaces of the hybrid CuO/PPy NCs with increased sizes become rougher than pure CuO NBs. Massive PPy nanoparticles are observed on the surface of hybrid CuO/PPy NCs, which are attributed to the gradual polymerization of pyrrole and the progressive deposition/coating of PPy nanoparticles on CuO NBs, along with extending polymerization time.

The detailed morphological structure features of CuO NBs and various CuO/PPy NCs were further examined by TEM. Figure 5a and e present TEM images of the overall CuO NBs and a typical CuO NB, respectively. Obviously, leaf-like CuO NBs have very smooth surfaces, and their widths and

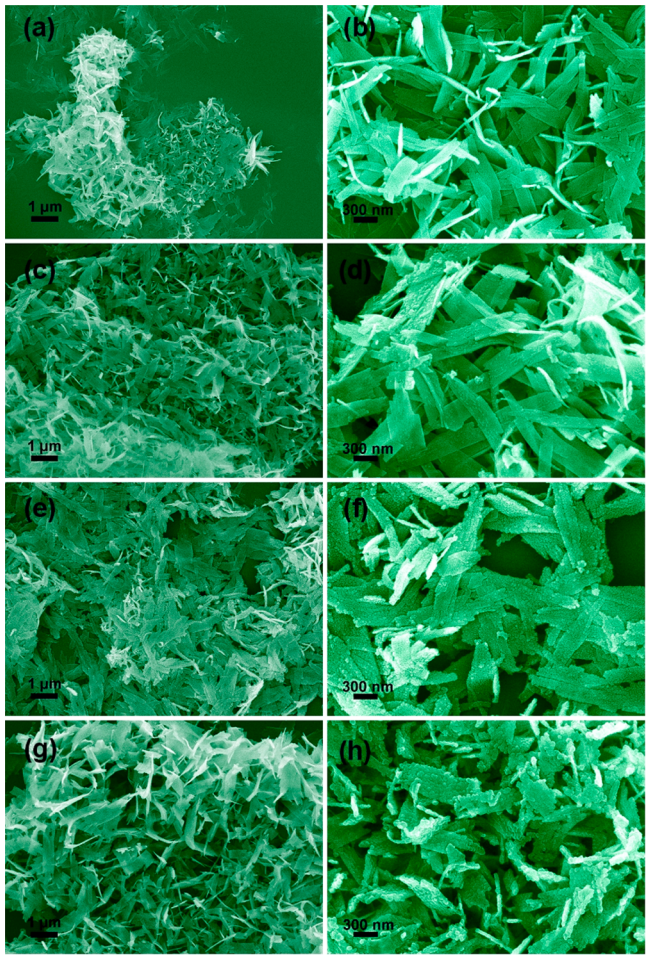


**Figure 4.** Low-magnification and high-magnification SEM images of the synthesized CuO NBs (a, b) and hybrid CuO/PPy NCs with controlled polymerization times: (c, d) 1 h, (e, f) 2 h, and (g, h) 3 h.

thicknesses are in the range of about 15−260 nm and 10−30 nm, respectively. These morphology and size results of CuO NBs determined by TEM are in agreement with of the SEM analysis. Moreover, the typical high-resolution TEM (HRTEM) image in Figure 5i exhibits a regular lattice spacing of 0.27 nm, which coincides well with the (110) planes of monoclinic CuO, implying that CuO NBs consist of single crystals and grow along the [010] direction. This agrees with earlier publications about the formation of CuO nanoribbons/rods/plates.[25,27,49] The selected area electron diffraction (SAED) pattern (inset) of a single CuO NB in Figure 5i further suggests that the formed monoclinic CuO NB consists of single crystal structures. Figure 5b, c, and d depict the detailed morphologies and structure features of CuO/PPy NCs synthesized by 1, 2, and 3 h polymerization, respectively. All these TEM images clearly show that the PPy modification on CuO NBs does not alter the overall profile of these products, whereas their surface roughnesses and sizes are increased. This indicates that PPy has been sufficiently modified on CuO NBs. Importantly, it is found that the polymerization time of pyrrole plays a significant role in affecting the final structure features of the hybrid products. Under 1 h polymerization, the resulting CuO/PPy NCs have 1D hybrid leaf-like NB structures, where organic PPy nanoparticles are distributed but not fully covered on the CuO surface (Figure 5f). With prolonged polymerization times of 2 and 3 h, the organic PPy shell layer is fully generated and


DOI: 10.1021/sc500755d
ACS Sustainable Chem. Eng. 2015, 3, 507−517

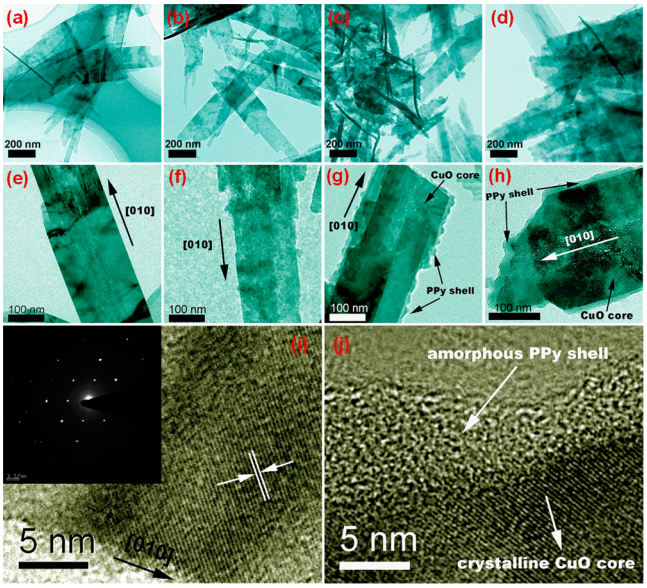


**Figure 5.** TEM images of CuO NBs (a) and hybrid CuO/PPy NCs with controlled polymerization times: (b) 1 h, (c) 2 h, and (d) 3 h. TEM images of a typical CuO NB (e) and typical CuO/PPy hybrid NBs derived from controlled polymerization times: (f) 1 h, (g) 2 h, and (h) 3 h. HRTEM images of the CuO NB (i) and the interface (j) between CuO and PPy in the hybrid NCs (3 h polymerization). Inset: SAED pattern of a single CuO NB.

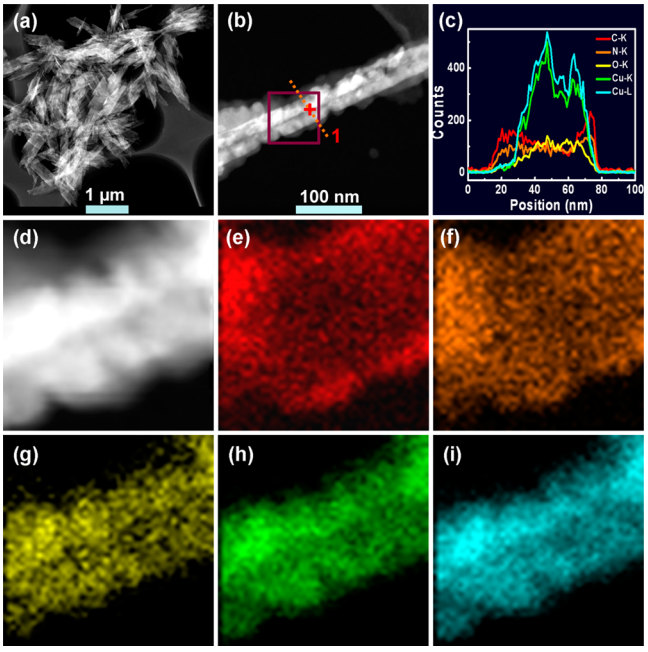


**Figure 6.** (a, b) STEM images of the hybrid CuO/PPy NCs synthesized by 3 h polymerization. (c) EDX line analysis of a single core–shell CuO/PPy NB along the line 1 in (b). EDX elemental mapping images of the square area (d) in a single core–shell CuO/PPy NB in panel (b): (e) C, (f) N, (g) O, and (h, i) Cu.

coated on CuO NBs, resulting in normal core–shell CuO/PPy composite nanoleaves (Figure 5g and h). When the polymerization time was controlled as 2 h, the thickness of the PPy sheath is about 5–25 nm with an average value of ~13 nm. When the time was further prolonged to 3 h, the coated shell thickness of PPy increases to about 8–45 nm (an average value of ~18 nm). Accordingly, the TEM results indicate that the microstructure features of hybrid CuO/PPy NCs and the shell thickness of the PPy layer can be facilely tuned by controlling the polymerization time of pyrrole. To further prove the formation of organic/inorganic core–shell nanostructures, the difference at the interface between the organic PPy shell and the inorganic CuO core is shown in Figure 5j. From this HRTEM image of a single CuO/PPy core–shell nanostructure made by 3 h polymerization, it can be found that an apparent PPy sheath layer with an amorphous structure is covered on the crystalline CuO core, which is consistent with the XRD characterization. Very importantly, the HRTEM result also reveals that there is an intimate interface interaction between the organic PPy and the inorganic CuO in the core–shell CuO/PPy NCs, which can make CuO electrochemically active because charge carriers could be effectively and rapidly conducted back and forth from CuO NBs to the current collector through the conducting polymer coating layers.[50] These results have clearly demonstrated that the normal core–shell CuO/PPy NCs are successfully achieved under the short polymerization time of only 2–3 h. Here, the phenomenon of polymerization time-dependent structure control is significant because most conducting polymer-derived NCs always require a longer polymerization process (e.g., 12 h or more).[38]

Furthermore, as shown in Figure 6, the structural features of the representative core–shell hybrid CuO/PPy NCs synthesized by 3 h polymerization have been confirmed by using STEM imaging and EDX linear analysis/elemental mapping. The presence and distribution of CuO and PPy in leaf-like core–shell NB were verified by EDX line analysis (Figure 6c). Along line 1 in Figure 6b, the strong Cu and O signals distributed in the middle position range of the single CuO/PPy NB confirm the CuO core, while the C and N signals surrounding the CuO core and also in the surface region clearly indicate the conjugation of PPy sheath layer on the CuO core. To further prove the presence of PPy sheath, EDX element mapping of the square area (Figure 6b and d) in a single core–shell CuO/PPy NB was utilized to detect the distribution of PPy in the hybrid CuO/PPy NCs. As displayed in Figure 6e–i, the color points are due to the presence of different elements within the hybrid CuO/PPy NCs. The C and N elements are present due to the formation of the PPy sheath, which is shown to be uniformly distributed in the core–shell CuO/PPy NC, along with Cu and O elements of the CuO core. It is found that the C, N, Cu and O in the sample are homogeneously distributed in the hybrid NB products, further demonstrating that conducting PPy is uniformly coated on the CuO surface, and the two components are connected well with each other. It is believed that the surface coating of conducting polymers on metal oxides can effectively enhance the electric conductivity of the metal oxide electrode materials and thus could be beneficial to Li storage.[38,42,43]

**Formation Mechanism of PPy-Modified CuO NCs.** The experimental flow and synthesis strategy for the formation of leaf-like CuO/PPy hybrid NCs is schematically illustrated in Figure 7. Briefly, the leaf-like CuO NBs are first synthesized in large-scale by a low-temperature (60 °C) water bath of $Cu(OH)_2$ precursors in a dilute NaOH solution. The generation of $Cu(OH)_2$ suspension is important for the solution phase growth of CuO crystallites, which initially serve as building blocks for the generation of the products.[47,51] Hence, at appropriate heating, many CuO nanocrystalline nuclei are produced during the dehydration process of


DOI: 10.1021/sc500755d
ACS Sustainable Chem. Eng. 2015, 3, 507–517

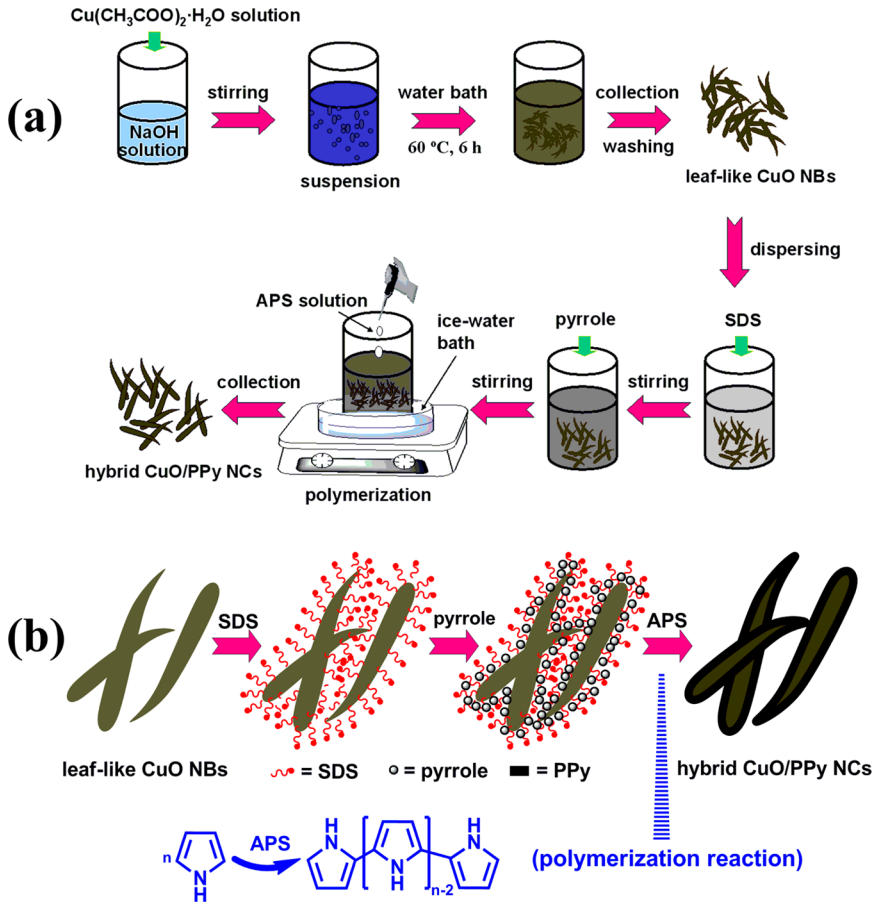


**Figure 7.** (a) Experimental flow diagram of synthesis of leaf-like CuO NBs and hybrid CuO/PPy NCs. (b) Schematic illustration for the wire template synthesis of core−shell CuO/PPy NCs.

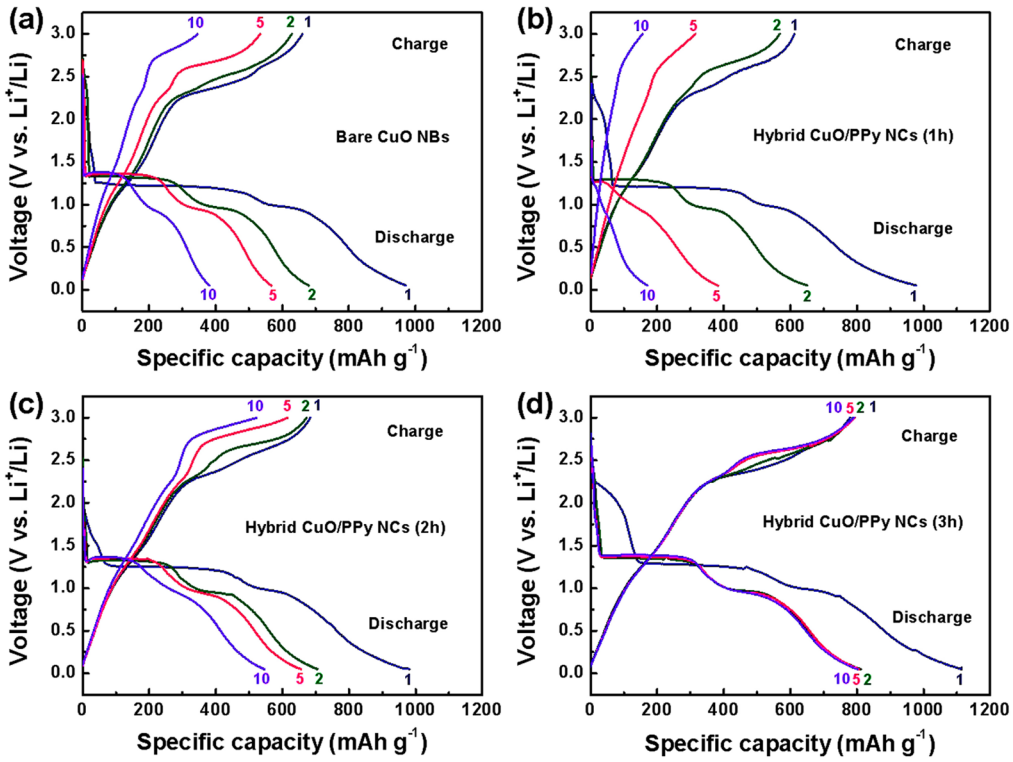


**Figure 8.** Discharge/charge curves at different cycles of bare CuO NBs (a) and different CuO/PPy NCs with controlled polymerization times (b−d). All the tests were taken between 0.05 and 3.0 V at 30 °C.



DOI: 10.1021/sc500755d
ACS Sustainable Chem. Eng. 2015, 3, 507−517

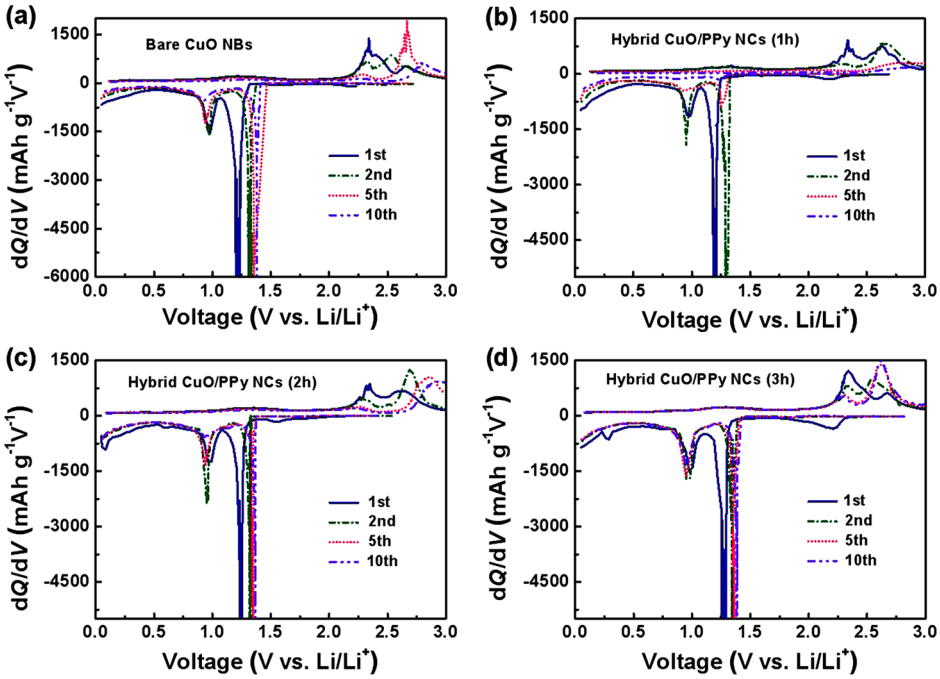


**Figure 9.** Differential capacity ($dQ/dV$) versus voltage plots of CuO NBs and different CuO/PPy NCs (synthesized by 1, 2, and 3 h polymerization) for the first, second, fifth, and tenth cycles.

$Cu(OH)_2$ precipitates in concentrated alkaline aqueous solution according to the reaction: $Cu(OH)_2 \xrightarrow{\Delta} CuO + H_2O$.[25] With continuous reaction at prolonged reaction time, $Cu(OH)_2$ converts into CuO crystals, and the formed crystals gradually grow in a 1D direction to result in NB structures. The one-pot formation of the final leaf-like CuO NBs can be attributed to the driving force provided by the Ostwald ripening and the basic environment, which are beneficial to the anisotropic growth of CuO nanocrystals.[27,47,49] Then, the synthesized leaf-like CuO NBs were collected, washed, and redispersed into deionized water as 1D wire templates for in situ synthesis of hybrid CuO/PPy NCs. Subsequently, a small amount of surfactant, SDS, is introduced to further disperse and modify CuO NBs in water. During synthesis, the wire templates of leaf-like CuO NBs can serve as physical scaffolds, while SDS molecules absorb on their surfaces and generate a soft interface.[43,45] After adding the pyrrole monomer and APS oxidant, chemical oxidation polymerization of the pyrrole occurs between the microarea of the soft SDS layer and the hard CuO core. Then, PPy is gradually polymerized and deposited on the CuO NB surface to form organic polymer coating layers. Finally, the normal core−shell CuO/PPy NCs are formed, where the controllable amount and sheath thickness of PPy can be tuned by controlling the polymerization time of pyrrole. Notably, the assistance of SDS is also an important factor in achieving high quality core−shell nanostructures. If SDS is not introduced to assist leaf-like CuO wire templates, the final CuO/PPy products did not show the core−shell structures. Their corresponding surface character is greatly different from that of the core−shell CuO/PPy NCs synthesized with SDS assistance, as evidenced by their amplified SEM image results (Figures S2 and S3, Supporting Information). It is anticipated that this synthetic strategy can be extended to the control synthesis of other polymer/metal oxide hybrids, especially for organic/inorganic core−shell composites.

**Electrochemical Lithium-Storage Properties of Samples.** The unique composite nanoleaf structures of organic/inorganic CuO-conducting polymer NCs make them promising materials for energy storage applications. Therefore, the electrochemical performance of these hybrid CuO/PPy NCs with different structural features as anode materials for LIBs are investigated. To evaluate their electrochemical lithium-storage properties, coin cells based on the synthesized samples were subjected to cyclic discharge/charge measurements. Figure 8 shows galvanostatic discharge−charge curves of the anodes based on bare CuO NBs and hybrid CuO/PPy NCs with varied polymerization times. Clearly, the discharge−charge profiles of CuO/PPy NCs are similar to those of CuO NBs, which indicates that the hybrid products modified by organic PPy do not change the lithium-storage nature of CuO anodes. Significantly, however, the discharge−charge properties of lithium storage have been significantly adjusted. In the case of CuO/PPy NCs synthesized by 1 h polymerization, the first discharge and charge capacities are 979 and 612 mAh $g^{-1}$ at a current density of 100 mA $g^{-1}$, respectively (Figure 8b). Due to the irreversible phase formation from the first charge, the second discharge capacity reduced to 652 mAh $g^{-1}$ and further dropped to 383 and 172 mAh $g^{-1}$ for the fifth and tenth cycles, respectively. In contrast to the anodes with bare CuO NBs, the lithium-storage capacity of this hybrid CuO/PPy NC (1 h) is not clearly improved (Figure 8a). This indicates that 1 h polymerization of pyrrole for hybrid CuO/PPy products is not sufficient to realize greatly improved lithium-storage performances. It may be attributed to the fact that there is no formation of doped-PPy shell structures on leaf-like NBs for CuO/PPy NCs (1 h), as determined by FT-IR, SEM, and TEM analysis. Conversely, by prolonging the polymerization time to 2 or 3 h, the resulting CuO/PPy NCs with core−shell structures exhibit remarkably enhanced lithium-storage capacities in contrast to hybrid CuO/PPy NCs without a normal PPy shell (1 h) and bare CuO NBs. As to core−shell CuO/PPy NCs synthesized


DOI: 10.1021/sc500755d
ACS Sustainable Chem. Eng. 2015, 3, 507−517

by 2 h polymerization, despite being tested at a higher current density (200 mA $g^{-1}$), the products can produce an enhanced discharge capacity of 982 mAh $g^{-1}$ (first cycle) and retain it at 705, 656, and 546 mAh $g^{-1}$ for the second, fifth, and tenth cycles, respectively (Figure 8c). For core−shell CuO/PPy NCs synthesized by 3 h polymerization, further improved discharge and charge capacities as high as 1114 and 779 mAh $g^{-1}$ (first cycle) are achieved, respectively, and also at a current density of 200 mA $g^{-1}$ (Figure 8d). Importantly, this anode still delivers high discharge (charge) capacities of 812 (788), 807 (794), and 802 (791) mAh $g^{-1}$ for the second, fifth, and tenth cycle, respectively. These lithium-storage capacities are much better than that of the CuO/PPy NCs reported earlier[43] and those data previously provided for nanostructured CuO anodes and commercial graphites in LIBs.[24,25,28,34,35,52] The practical capacities of these CuO/PPy and CuO products are also larger than the theoretical capacity of 674 mAh $g^{-1}$ based on a maximum uptake of 2Li/CuO. The extra capacity can be attributed to the decomposition of electrolyte and the reversible formation of a polymer gel-like film on the surface of the particles that occurs in the low potential region.[25,29,30,53] Considering that pure PPy does not contribute to the anode capacity,[41] it is thus mainly taking the role of conducting and buffering CuO with its effective surface modification. Accordingly, these results demonstrate that facile formation and structural optimization of core−shell CuO/PPy NCs by controlling the polymerization time of pyrrole can greatly improve the lithium-storage capacity of CuO NCs in LIBs.

The lithium storage mechanism of the CuO anodes has been proposed as the multistep electrochemical reactions of CuO with Li.[18,19,29,30,43] To illustrate the redox characteristics of synthesized CuO NBs and CuO/PPy NCs, differential capacity versus voltage ($dQ/dV$) plots of the first, second, fifth, and tenth cycles of all the samples are displayed in Figure 9. In the first discharge process, three reduction peaks are observed at near 2.1 V (wide), 1.2 V (strong), and 0.97 V (moderate) on the samples, which are ascribed to the multistep electrochemical reductions of CuO with Li intercalation (formation of a $Cu^{II}_{1-x}Cu^{I}_{x}O_{1-x/2}$ ($0 \le x \le 0.4$) solid solution, creation of a $Cu_2O$ phase, and decomposition of $Cu_2O$ into $Li_2O$ and Cu).[18,19,29,43] In the first charge process, two oxidation peaks at approximately 2.3 V (strong) and 2.7 V (moderate) can be observed on all the samples, corresponding to the Li-extraction process $2Cu+Li_2O \rightarrow Cu_2O+2Li$ and the partial oxidation of $Cu_2O$ into CuO.[30,43] From the second cycle onward, the reduction and oxidation potentials are shifted to some extent. The changes of peak potentials and intensities in redox curves imply the irreversible capacities of products during the first and second cycles, which are consistent with the observation in the above discharge/charge curves. In the subsequent cycles, the overlapping of redox curves in the core−shell CuO/PPy NCs (2 and 3 h) suggests their good electrochemical activity and reversibility, as well as structural stability. By comparison, those redox peaks of CuO/PPy NCs (1 h) without PPy shell structures have a noticeable decline in peak intensity, indicating their severe capacity fading under cycling similar to that of bare CuO NBs. The substantial decreases in main peak intensity and integral area of hybrid CuO/PPy NCs (1 h) in the next cycles designate that there are larger reversible capacity losses for them as compared with those of core−shell CuO/PPy NCs (2 and 3 h).

**Cyclic Stability of Samples.** To further investigate the effect of the material structures on lithium storage, the cycling performance of CuO NBs and different CuO/PPy NCs made by the controlled polymerization time is also compared in Figure 10. Obviously, the cyclic performance of hybrid CuO/PPy NCs is gradually improved with prolonging the polymerization time of pyrrole from 1 to 3 h. As shown in Figure 10a, hybrid CuO/PPy NC anodes with core−shell nanostructures (2 and 3 h polymerization) exhibit much better cyclic stability than that of CuO/PPy NCs without core−shell structures (1 h polymerization) and pure CuO NBs. For optimized core−shell CuO/PPy NCs made by 3 h polymerization, they can retain a high reversible capacity of 760 mAh $g^{-1}$ over 45 cycles, which is the best cyclic performance among all synthesized NCs in this work. Similarly, core−shell CuO/PPy NCs made by 2 h polymerization also maintain a high capacity of 518 mAh $g^{-1}$ over 45 cycles. By contrast, the capacities of CuO/PPy NCs (1 h) without core−shell structures and bare CuO NBs fade quickly to only 79 and 110 mAh $g^{-1}$ after 20 cycles, respectively, even under a half current density (100 mA $g^{-1}$). With longer cycling tests, the discharge/charge curves for the 85th and 110th cycles of CuO/PPy (2 and 3 h) still show much better performance than that of CuO/PPy (1 h) and CuO (Figure S4, Supporting Information), further demonstrating that core−shell hybrids enhance performance in contrast to structures without core−shell features. The improved performance for core−shell structures is mainly benefited from the PPy shell, which buffers volume variations of CuO and prevents cracked CuO fragments from being extracted into the electryte.[54] Figure 10b further displays Coulombic efficiencies of the various samples during the cyclic discharge/charge

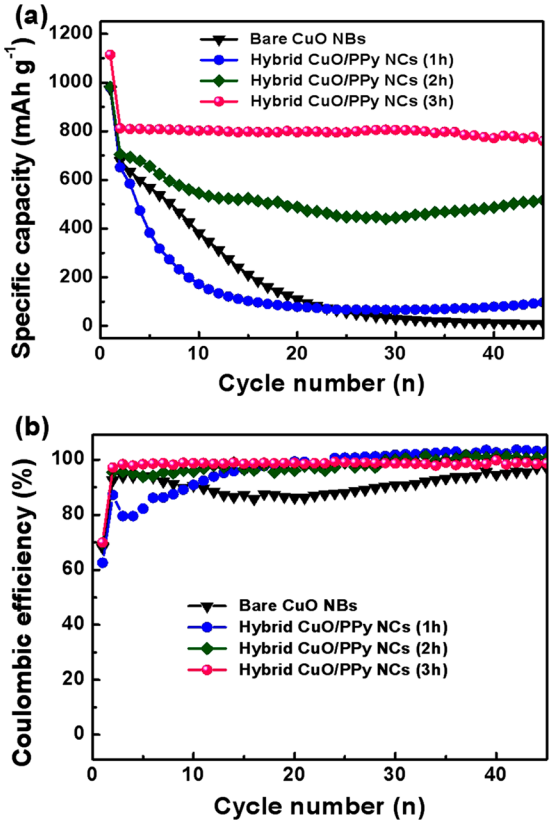


**Figure 10.** Comparative cycling performances of CuO NBs and different CuO/PPy NCs with controlled polymerization times. All tests were taken between 0.05 and 3.0 V at 30 °C.


DOI: 10.1021/sc500755d
ACS Sustainable Chem. Eng. 2015, 3, 507−517

processes. The first Coulombic efficiencies of bare CuO NBs and different CuO/PPy NCs with 1, 2, and 3 h polymerization are 68.0%, 62.5%, 69.7%, and 69.9%, respectively. These low initial Coulombic efficiencies mean that the large capacity losses between the discharge and charge in the first cycle exist in all these anode materials. The reasons are the formation of a solid electrolyte interface (SEI) layer on the surfaces of active electrode materials, partly irreversible lithium oxide in metal oxide anodes, and possible phase transition of electrodes.[42,55] As further shown, both anodes of the core−shell CuO/PPy NCs (2 and 3 h) show high Coulombic efficiencies (≥93.9%) in the succeeding cyclic processes, which are superior or similar to those of CuO/PPy NCs without core−shell structures (1 h). The high Coulombic efficiencies are also much better than those of bare CuO NB anodes.

Here, the improved lithium-storage capacities, enhanced cyclic performances, and high Coulombic efficiencies of core−shell CuO/PPy NCs are attributed to the unique structure features of the metal oxide/conducting polymer core−shell hybrid products. In this architecture, the stable and flexible PPy sheath can buffer the structural variation of rigid CuO NBs during charging/discharging processes and prevent the pulverization of CuO NBs, as well as protect CuO from direct contact with electrolytes and prohibit irreversible side reactions.[38,41,43,56,57] Meanwhile, good interfacial interaction between the conductive PPy sheath and CuO core in the core−shell CuO/PPy composites improves the utilization of active CuO for Li storage and allows them to be efficient electrodes to promote charge transfer processes in LIBs.[50,58] The solid CuO core and flexible PPy shell prevent, synergistically, the hybrid composite nanoleaves from significant collapsing, pulverizing, and breaking, which greatly improves their mechanical stability.[59] The mechanical stability is also enhanced by the thin-film effect combined with PPy coating on the hybrids, which plays a structural buffering role in minimizing the mechanical stress induced by the volume change of CuO.[54] Thereby the 1D CuO/PPy core−shell hybrid NCs provide a stable environment and short ion diffusion paths for $Li^+$ intercalation/extraction due to their mechanical flexibility, stability, and good conductivity. The ability to accommodate volume variations of electrodes as well as to facilitate effective Li-ion diffusion and charge-transport, leads to eventual good electrochemical lithium-storage capacity and cycling durability over repeated discharge/charge cycles. Whereas, the lower capacities and faster capacity fading of bare CuO NBs may result from their pulverization and aggregation under the cycling. As to CuO/PPy NCs without core−shell features, the poor cyclic performance is similar to that of the bare CuO NBs because doped PPy has not fully formed and coated on CuO NBs made by 1 h polymerization.

## CONCLUSION

In summary, composite nanoleaves of PPy-modified CuO with various shell structures have been successfully synthesized. The results demonstrate that the polymerization time of pyrrole acts as a significant role in affecting both the structure features and lithium-storage properties of the hybrid CuO/PPy NCs. By prolonging the polymerization time, the CuO/PPy NC products progressively form typical core−shell structures, where the doped PPy shell with increasing amounts is steadily and uniformly coated on the CuO surface. The formation of organic/inorganic core−shell nanostructures of CuO/PPy NCs is important for achieving enhanced lithium-storage capacities, good cyclic stabilities, and high Coloumbic efficiencies. When used as promising anode materials for LIBs, the core−shell CuO/PPy NCs exhibit much higher discharge/charge capacities and better cycling performance compared to CuO/PPy NCs without core−shell features and pure CuO NBs. The optimized core−shell CuO/PPy NCs can deliver a greatly improved initial capacity of 1114 mAh $g^{-1}$ and retain a high reversible value of 760 mAh $g^{-1}$ after 45 cycles. The enhanced performance of this type of hybrid nanoleaf materials is due to their advantageous structure features. This work provides a facile and effective pathway for surface modification of metal oxides by in situ polymerization of conducting polymers, which is crucial to enhance Li-storage properties in LIBs. The shell structure control and structure−property relationships of these CuO/PPy NCs can be guidelines for other polymer-based composites for energy storage applications.

## ASSOCIATED CONTENT

### Supporting Information

EDX spectrum of the bare CuO sample, SEM images, and discharge/charge curves of different CuO/PPy samples. This material is available free of charge via the Internet at http://pubs.acs.org.

## AUTHOR INFORMATION

### Corresponding Authors

*E-mail:guanlh@fjirsm.ac.cn. Tel: +86 591 83721625. Fax: +86 591 83721625.

*E-mail:qingdongzheng@fjirsm.ac.cn. Tel: +86 591 83721625. Fax: +86 591 83721625.

### Notes

The authors declare no competing financial interest.

## ACKNOWLEDGMENTS

This work was financially supported by the National Natural Science Foundation of China (51203158 and 61325026), National Basic Research 973 Program (2011CB935904), Natural Science Foundation of Fujian Province (2014J01216), CAS/SAFEA International Partnership Program for Creative Research Teams, and 100 Talents Programme of the Chinese Academy of Sciences.

## REFERENCES

(1) Cheng, F. Y.; Liang, J.; Tao, Z. L.; Chen, J. Functional materials for rechargeable batteries. *Adv. Mater.* **2011**, *23*, 1695−1715.

(2) Espinoza, V. S.; Erbis, S.; Pourzahedi, L.; Eckelman, M. J.; Isaacs, J. A. Material flow analysis of carbon nanotube lithium-ion batteries used in portable computers. *ACS Sustainable Chem. Eng.* **2014**, *2*, 1642−1648.

(3) Arico, A. S.; Bruce, P.; Scrosati, B.; Tarascon, J. M.; Van Schalkwijk, W. Nanostructured materials for advanced energy conversion and storage devices. *Nat. Mater.* **2005**, *4*, 366−377.

(4) Chung, S.-H.; Manthiram, A. Eggshell-membrane-derived polysulfide absorbents for highly stable and reversible lithium-sulfur cells. *ACS Sustainable Chem. Eng.* **2014**, *2*, 2248−2252.

(5) Wang, Y.; Cao, G. Z. Developments in nanostructured cathode materials for high-performance lithium-ion batteries. *Adv. Mater.* **2008**, *20*, 2251−2269.

(6) Liu, C.; Li, F.; Ma, L. P.; Cheng, H. M. Advanced materials for energy storage. *Adv. Mater.* **2010**, *22*, E28−E62.

(7) Xin, S.; Guo, Y. G.; Wan, L. J. Nanocarbon networks for advanced rechargeable lithium batteries. *Acc. Chem. Res.* **2012**, *45*, 1759−1769.



DOI: 10.1021/sc500755d
*ACS Sustainable Chem. Eng.* 2015, 3, 507−517

(8) Tarascon, J. M.; Armand, M. Issues and challenges facing rechargeable lithium batteries. *Nature* **2001**, *414*, 359−367.
(9) Armand, M.; Tarascon, J. M. Building better batteries. *Nature* **2008**, *451*, 652−657.
(10) Ji, X. L.; Lee, K. T.; Nazar, L. F. A highly ordered nanostructured carbon-sulphur cathode for lithium-sulphur batteries. *Nat. Mater.* **2009**, *8*, 500−506.
(11) Chen, H. X.; Xiao, Y.; Wang, L.; Yang, Y. Silicon nanowires coated with copper layer as anode materials for lithium-ion batteries. *J. Power Sources* **2011**, *196*, 6657−6662.
(12) Poizot, P.; Laruelle, S.; Grugeon, S.; Dupont, L.; Tarascon, J. M. Nano-sized transition-metaloxides as negative-electrode materials for lithium-ion batteries. *Nature* **2000**, *407*, 496−499.
(13) Jiang, J.; Li, Y. Y.; Liu, J. P.; Huang, X. T.; Yuan, C. Z.; Lou, X. W. Recent advances in metal oxide-based electrode architecture design for electrochemical energy storage. *Adv. Mater.* **2012**, *24*, 5166−5180.
(14) Reddy, M. V.; Rao, G. V. S.; Chowdari, B. V. R. Metal oxides and oxysalts as anode materials for Li ion batteries. *Chem. Rev.* **2013**, *113*, 5364−5457.
(15) Wang, N.; Chen, L.; Ma, X.; Yue, J.; Niu, F.; Xu, H.; Yang, J.; Qian, Y. Facile synthesis of hierarchically porous NiO micro-tubes as advanced anode materials for lithium-ion batteries. *J. Mater. Chem. A* **2014**, *2*, 16847−16850.
(16) Yue, J.; Gu, X.; Chen, L.; Wang, N.; Jiang, X.; Xu, H.; Yang, J.; Qian, Y. General synthesis of hollow $MnO_2$, $Mn_3O_4$ and MnO nanospheres as superior anode materials for lithium ion batteries. *J. Mater. Chem. A* **2014**, *2*, 17421−17426.
(17) Chen, L.; Xu, H.; Li, L.; Wu, F.; Yang, J.; Qian, Y. A comparative study of lithium-storage performances of hematite: Nanotubes vs. nanorods. *J. Power Sources* **2014**, *245*, 429−435.
(18) Debart, A.; Dupont, L.; Poizot, P.; Leriche, J. B.; Tarascon, J. M. A transmission electron microscopy study of the reactivity mechanism of tailor-made CuO particles toward lithium. *J. Electrochem. Soc.* **2001**, *148*, A1266−A1274.
(19) Morales, J.; Sanchez, L.; Martin, F.; Ramos-Barrado, J. R.; Sanchez, M. Nanostructured CuO thin film electrodes prepared by spray pyrolysis: a simple method for enhancing the electrochemical performance of CuO in lithium cells. *Electrochim. Acta* **2004**, *49*, 4589−4597.
(20) Yuan, C. Z.; Wu, H. B.; Xie, Y.; Lou, X. W. Mixed transition-metal oxides: design, synthesis, and energy-related applications. *Angew. Chem., Int. Ed.* **2014**, *53*, 1488−1504.
(21) Oh, S. W.; Bang, H. J.; Bae, Y. C.; Sun, Y. K. Effect of calcination temperature on morphology, crystallinity and electrochemical properties of nano-crystalline metal oxides ($Co_3O_4$, CuO, and NiO) prepared via ultrasonic spray pyrolysis. *J. Power Sources* **2007**, *173*, 502−509.
(22) Xiang, J. Y.; Tu, J. P.; Zhang, L.; Zhou, Y.; Wang, X. L.; Shi, S. J. Self-assembled synthesis of hierarchical nanostructured CuO with various morphologies and their application as anodes for lithium ion batteries. *J. Power Sources* **2010**, *195*, 313−319.
(23) Wang, C.; Li, Q.; Wang, F.; Xia, G.; Liu, R.; Li, D.; Li, N.; Spendelow, J. S.; Wu, G. Morphology-dependent performance of CuO anodes via facile and controllable synthesis for lithium-ion batteries. *ACS Appl. Mater. Interfaces* **2014**, *6*, 1243−1250.
(24) Park, J. C.; Kim, J.; Kwon, H.; Song, H. Gram-scale synthesis of $Cu_2O$ nanocubes and subsequent oxidation to CuO hollow nanostructures for lithium-ion battery anode materials. *Adv. Mater.* **2009**, *21*, 803−807.
(25) Gao, X. P.; Bao, J. L.; Pan, G. L.; Zhu, H. Y.; Huang, P. X.; Wu, F.; Song, D. Y. Preparation and electrochemical performance of polycrystalline and single crystalline CuO nanorods as anode materials for Li ion battery. *J. Phys. Chem. B* **2004**, *108*, 5547−5551.
(26) Chen, L. B.; Lu, N.; Xu, C. M.; Yu, H. C.; Wang, T. H. Electrochemical performance of polycrystalline CuO nanowires as anode material for Li ion batteries. *Electrochim. Acta* **2009**, *54*, 4198−4201.
(27) Zou, G. F.; Li, H.; Zhang, D. W.; Xiong, K.; Dong, C.; Qian, Y. T. Well-aligned arrays of CuO nanoplatelets. *J. Phys. Chem. B* **2006**, *110*, 1632−1637.
(28) Zhang, D. W.; Yi, T. H.; Chen, C. H. Cu nanoparticles derived from CuO electrodes in lithium cells. *Nanotechnology* **2005**, *16*, 2338−2341.
(29) Zhang, W. X.; Li, M.; Wang, Q.; Chen, G. D.; Kong, M.; Yang, Z. H.; Mann, S. Hierarchical self-assembly of microscale cog-like superstructures for enhanced performance in lithium-ion batteries. *Adv. Funct. Mater.* **2011**, *21*, 3516−3523.
(30) Wang, S. Q.; Zhang, J. Y.; Chen, C. H. Dandelion-like hollow microspheres of CuO as anode material for lithium-ion batteries. *Scripta. Mater.* **2007**, *57*, 337−340.
(31) Sahay, R.; Kumar, P. S.; Aravindan, V.; Sundaramurthy, J.; Ling, W. C.; Mhaisalkar, S. G.; Ramakrishna, S.; Madhavi, S. High aspect ratio electrospun CuO nanofibers as anode material for lithium-ion batteries with superior cycleability. *J. Phys. Chem. C* **2012**, *116*, 18087−18092.
(32) Chen, X.; Zhang, N. Q.; Sun, K. N. Facile fabrication of CuO 1D pine-needle-like arrays for super-rate lithium storage. *J. Mater. Chem.* **2012**, *22*, 15080−15084.
(33) Wang, L. L.; Gong, H. X.; Wang, C. H.; Wang, D. K.; Tang, K. B.; Qian, Y. T. Facile synthesis of novel tunable highly porous CuO nanorods for high rate lithium battery anodes with realized long cycle life and high reversible capacity. *Nanoscale* **2012**, *4*, 6850−6855.
(34) Zheng, S. F.; Hu, J. S.; Zhong, L. S.; Song, W. G.; Wan, L. J.; Guo, Y. G. Introducing dual functional CNT networks into CuO nanomicrospheres toward superior electrode materials for lithium-ion batteries. *Chem. Mater.* **2008**, *20*, 3617−3622.
(35) Wang, B.; Wu, X. L.; Shu, C. Y.; Guo, Y. G.; Wang, C. R. Synthesis of CuO/graphene nanocomposite as a high-performance anode material for lithium-ion batteries. *J. Mater. Chem.* **2010**, *20*, 10661−10664.
(36) Huang, X. H.; Wang, C. B.; Zhang, S. Y.; Zhou, F. CuO/C microspheres as anode materials for lithium ion batteries. *Electrochim. Acta* **2011**, *56*, 6752−6756.
(37) Ko, S.; Lee, J. I.; Yang, H. S.; Park, S.; Jeong, U. Mesoporous CuO particles threaded with CNTs for high-performance lithium-ion battery anodes. *Adv. Mater.* **2012**, *24*, 4451−4456.
(38) Yin, Z. G.; Zheng, Q. D. Controlled synthesis and energy applications of one-dimensional conducting polymer nanostructures: An overview. *Adv. Energy Mater.* **2012**, *2*, 179−218.
(39) Huang, X. H.; Tu, J. P.; Xia, X. H.; Wang, X. L.; Xiang, J. Y. Nickel foam-supported porous NiO/polyaniline film as anode for lithium ion batteries. *Electrochem. Commun.* **2008**, *10*, 1288−1290.
(40) Liu, R.; Duay, J.; Lee, S. B. Redox exchange induced $MnO_2$ nanoparticle enrichment in poly(3,4-ethylenedioxythiophene) nanowires for electrochemical energy storage. *ACS Nano* **2010**, *4*, 4299−4307.
(41) Cui, L. F.; Shen, J. A.; Cheng, F. Y.; Tao, Z. L.; Chen, J. $SnO_2$ nanoparticles@polypyrrole nanowires composite as anode materials for rechargeable lithium-ion batteries. *J. Power Sources* **2011**, *196*, 2195−2201.
(42) Zhao, J. F.; Zhang, S. C.; Liu, W. B.; Du, Z. J.; Fang, H. $Fe_3O_4$/PPy composite nanospheres as anode for lithium-ion batteries with superior cycling performance. *Electrochim. Acta* **2014**, *121*, 428−433.
(43) Yin, Z. G.; Ding, Y. H.; Zheng, Q. D.; Guan, L. H. CuO/polypyrrole core-shell nanocomposites as anode materials for lithium-ion batteries. *Electrochem. Commun.* **2012**, *20*, 40−43.
(44) Cho, G. J.; Fung, B. M.; Glatzhofer, D. T.; Lee, J. S.; Shul, Y. G. Preparation and characterization of polypyrrole-coated nanosized novel ceramics. *Langmuir* **2001**, *17*, 456−461.
(45) Lu, X. F.; Mao, H.; Zhang, W. J. Surfactant directed synthesis of polypyrrole/$TiO_2$ coaxial nanocables with a controllable sheath size. *Nanotechnology* **2007**, *18*, 025604.
(46) Zhong, W. B.; Liu, S. M.; Chen, X. H.; Wang, Y. X.; Yang, W. T. High-yield synthesis of superhydrophilic polypyrrole nanowire networks. *Macromolecules* **2006**, *39*, 3224−3230.
(47) Vaseem, M.; Umar, A.; Kim, S. H.; Hahn, Y. B. Low-temperature synthesis of flower-shaped CuO nanostructures by solution process: formation mechanism and structural properties. *J. Phys. Chem. C* **2008**, *112*, 5729−5735.


DOI: 10.1021/sc500755d
*ACS Sustainable Chem. Eng.* 2015, 3, 507−517

(48) Hwang, J. K.; Lim, H. S.; Sun, Y. K.; Suh, K. D. Monodispersed hollow carbon/$Fe_3O_4$ composite microspheres for high performance anode materials in lithium-ion batteries. *J. Power Sources* **2013**, *244*, 538−543.
(49) Liu, B.; Zeng, H. C. Mesoscale organization of CuO nanoribbons: formation of ″dandelions″. *J. Am. Chem. Soc.* **2004**, *126*, 8124−8125.
(50) Wang, H. L.; Cui, L. F.; Yang, Y. A.; Casalongue, H. S.; Robinson, J. T.; Liang, Y. Y.; Cui, Y.; Dai, H. J. $Mn_3O_4$-graphene hybrid as a high-capacity anode material for lithium ion batteries. *J. Am. Chem. Soc.* **2010**, *132*, 13978−13980.
(51) Yin, Z.; Wang, B.; Chen, G.; Zhan, M. One-dimensional 8-hydroxyquinoline metal complex nanomaterials: Synthesis, optoelectronic properties, and applications. *J. Mater. Sci.* **2011**, *46*, 2397−2409.
(52) Xu, M. W.; Wang, F.; Ding, B. J.; Song, X. P.; Fang, J. X. Electrochemical synthesis of leaf-like CuO mesocrystals and their lithium storage properties. *RSC Adv.* **2012**, *2*, 2240−2243.
(53) Laruelle, S.; Grugeon, S.; Poizot, P.; Dollé, M.; Dupont, L.; Tarascon, J. M. On the origin of the extra electrochemical capacity displayed by MO/Li cells at low potential. *J. Electrochem. Soc.* **2002**, *149*, A627−A634.
(54) Liang, B.; Liu, Y.; Xu, Y. Silicon-based materials as high capacity anodes for next generation lithium ion batteries. *J. Power Sources* **2014**, *267*, 469−490.
(55) Zhang, Q. M.; Shi, Z. C.; Deng, Y. F.; Zheng, J.; Liu, G. C.; Chen, G. H. Hollow $Fe_3O_4$/C spheres as superior lithium storage materials. *J. Power Sources* **2012**, *197*, 305−309.
(56) Han, F.; Li, D.; Li, W. C.; Lei, C.; Sun, Q.; Lu, A. H. Nanoengineered polypyrrole-coated $Fe_2O_3$@C multifunctional composites with an improved cycle stability as lithium-ion anodes. *Adv. Funct. Mater.* **2013**, *23*, 1692−1700.
(57) Mao, Y.; Kong, Q. Y.; Guo, B. K.; Shen, L.; Wang, Z. X.; Chen, L. Q. Polypyrrole-NiO composite as high-performance lithium storage material. *Electrochim. Acta* **2013**, *105*, 162−169.
(58) Wu, Z. S.; Zhou, G. M.; Yin, L. C.; Ren, W.; Li, F.; Cheng, H. M. Graphene/metal oxide composite electrode materials for energy storage. *Nano Energy* **2012**, *1*, 107−131.
(59) Liu, R.; Lee, S. B. $MnO_2$/poly(3,4-ethylenedioxythiophene) coaxial nanowires by one-step coelectrodeposition for electrochemical energy storage. *J. Am. Chem. Soc.* **2008**, *130*, 2942−2943.


DOI: 10.1021/sc500755d
*ACS Sustainable Chem. Eng.* 2015, 3, 507−517